Journal of Power Sources 264 (2014) 184–194

Contents lists available at ScienceDirect

Journal of Power Sources

journal homepage: www.elsevier.com/locate/jpowsour

Mathematical model of lithium-ion batteries with blended-electrode system

Seunghun Jung*

Battery R&D, LG Chem Research Park, 104-1, Moonji-dong, Yuseong-gu, Daejeon 305-380, Republic of Korea

HIGHLIGHTS

- Two mathematical models of lithium-ion cell with blended-electrodes are developed.
- Equilibrium model can easily calculate equilibrium characteristics of a blended-electrode.
- Dynamic model can predict dynamic performance of a lithium-ion cell with blended-electrodes.
- Developed model is validated with experiment data and shows good agreements.

ARTICLE INFO

Article history:
Received 12 March 2014
Received in revised form
14 April 2014
Accepted 15 April 2014
Available online 26 April 2014

Keywords:
Lithium-ion
Battery
Blended electrode
Mixed electrode
Modeling

ABSTRACT

Many lithium-ion batteries have electrodes made of multiple types of active materials in order to take advantage of each active material. According to the types and blending ratios of constituting active materials, there can be numerous combinations of blended-electrodes, resulting in different performance characteristics. This paper introduces how to numerically model lithium-ion batteries with blended-electrodes, and predict their performance. Further, this paper demonstrates how to apply the developed model to designing new batteries. First, we propose an equilibrium model which can predict equilibrium characteristics of a blended-electrode. Second, a physics-based lithium-ion cell model with blended-electrodes is proposed. Developed model is validated with experimental data and shows good agreements.

1. Introduction

Although lithium-ion batteries commercialized by SONY have several merits such as larger capacity, lighter weight, and good coulombic efficiency compared to previously used batteries of other chemistry such as nickel-metal hydride batteries, there has been doubt that lithium-ion battery is not safe enough to be used for automotive power source. However, recently, lithium-ion battery is getting much more public, industrial attention. Several automakers have launched hybrid electric vehicles (HEV), plug-in hybrid electric vehicles (PHEV), and battery electric vehicles (BEV) powered by lithium-ion batteries after GM successfully launched the first commercialized plug-in hybrid vehicle, VOLT™ which loads LG Chem's high performance lithium-ion batteries. In contrast to small batteries for portable electronics, automotive lithium-ion batteries must sustain severe operating conditions and requirements. Therefore, it requires much more time and efforts to develop large-formatted automotive batteries than small batteries for mobile applications.

Typical lithium-ion batteries are composed of negative active materials, positive active materials, electrolyte, separator, additives, and current collectors. Active materials are the most important among them since they determine power and energy of a battery. Many negative and positive active materials have been searched up to now and each of active material has its own characteristics such as operating potential profile, capacity and power. For example, $LiMn_2O_4$ has good rate capability and high power with relatively low cost and less safety problem. But, it shows low capacity and Manganese (Mn) dissolution problem also. In contrast, Li(Ni, Mn, Co)O_2 has more capacity compared to $LiMn_2O_4$, but shows lower power due to the layered structure and lower operating potential window. Olivine material such as $LiFePO_4$ is considered as one of promising positive materials due to low cost, improved safety with large capacity. Many researches to overcome low electronic

* Tel.: +82 42 866 2094; fax: +82 42 862 1981.
E-mail address: stratus76@hotmail.com.

http://dx.doi.org/10.1016/j.jpowsour.2014.04.072
0378-7753/

conductivity and very low lithium diffusion rate of $LiFePO_4$ (briefly 'LFP') particle have been conducted [1–4]. As briefly listed above, most of active material have both merits and demerits together. Therefore, it is important to select proper active materials for specified purposes. Since large battery capacity is the most important factor for full electric vehicles (EV), $Li(Ni_{1/3}Mn_{1/3}Co_{1/3})O_2$ (briefly 'NMC') can be selected as positive active material and graphite can be used for negative electrode. In contrast, high power is the most required quality for hybrid electric cars (HEV). In this case, spinel materials such as $LiMn_2O_4$ (briefly 'LMO') and amorphous materials such as carbon can be adopted for positive electrode and negative electrode, respectively. When both capacity and power are important, multiple active materials can be blended together, so called 'blended-electrode'.

Several papers about experimental work on blended-electrodes have been published. Mitigating Manganese dissolution and improving capacity retention by blending different active materials together were considered important by several researchers [5–7]. Fergus [8] extensively reviewed cathode materials including composite electrodes. He categorized electrode with different mixed particles and electrodes with coated particles layered as composite electrode. Whitacre et al. [9] constructed fully mixed (blended) electrodes, fully segregated electrodes and layered electrodes by using $LiFePO_4$ and $Li(Li_{0.17}Mn_{0.58}Ni_{0.25})O_2$. They tried to take advantages of composite electrode from each active material (high rate capability of $LiFePO_4$ and large capacity of $Li(Li_{0.17}Mn_{0.58}Ni_{0.25})O_2$ and they found that segregated active material configuration is the most promising solution with those two active materials.

As briefly reviewed above, it is worthwhile to consider blending several active materials together to improve cell performance. However, blending different active materials may cause some problems in a complex slurry mixing process or electrode coating process, which may result in increased manufacturing cost. In addition, much time and cost would be required to find optimum blending ratio for target performance of a cell. Actually, it takes much time and cost to finalize cell chemistry because cell makers go through several screening tests for candidate materials. Further, numerous new active materials are being introduced by material makers. Although, it is good for cell makers to have many options to choose, required time and cost for a new cell development may increase as the combination number of materials grows larger. If the performance of a new cell with blended-electrodes can be mathematically predicted before the actual cell is constructed, cell development cost will be significantly saved.

Few publications about modeling work on blended electrodes can be found up to now. Darling and Newman [10] started a modeling work on the electrode with two distinct particle sizes. Gomadam et al. [11] developed a mathematical model simulating a composite electrode made of carbon monofluoride (CF_x) and silver vanadium oxide (SVO) for medical applications. Although their model is relatively simplified with many assumptions, their modeling result showed good agreement with the experimental result from a small half cell test within moderate C-rate discharging condition. Albertus et al. [15–17] conducted more extensive modeling work on blended electrodes. They modified their mathematical cell model to treat electrodes made of multiple types of active particles, and simulated several composition of two types of active materials ($LiNi_{0.80}Co_{0.15}Al_{0.05}O_2$ and $LiMn_2O_4$). They presented that their blended electrode showed combined characteristics (such as power and energy) of each pure active material. Jung and Kang [18] introduced a multi-dimensional model of lithium-ion cells with blended-electrodes. But, their model was an empirical model which could not be used to predict characteristics of a lithium-ion cell without actual experiment data.

This paper introduces how to predict performance of lithium-ion batteries with blended-electrodes by mathematical method. First, we introduce the blended-electrode model in equilibrium state, which is useful to predict open-circuit voltage of a blended-electrode with arbitrary combinations of multiple active materials. Second, the physics-based dynamic model is explained, which can simulate battery performance in dynamic operating conditions and explain physico-chemical phenomena inside blended-electrodes.

2. Equilibrium model

A pure active material has a distinct equilibrium voltage profile according to lithium intercalation level or lithium stoichiometry, which can be used for us to predict charging/discharging characteristics of a cell made of the active material. By combining such equilibrium voltage data of several active materials, it is possible to predict basic characteristics such as discharging profile of a blended-electrode as follows.

Fig. 1 represents equilibrium voltage profiles of basic active materials for this study. The basic concept of the present equilibrium model of a blended-electrode is that the blended-electrode is in thermodynamically equilibrium state. In other words, the surface energy level (or the potential) of the constituting active particles should remain same level by minimizing potential difference between active particles. This causes each different active particle may have different state of charge (lithium stoichiometry) under equilibrium condition of the blended-electrode. Therefore, we can find out state of charge (lithium stoichiometry) of each constituting active material. Theoretical capacity of $LiMn_2O_4$ is about 150 mAh g^{-1} while usable capacity is about 107 mAh g^{-1} (150–107 = 43 mAh g^{-1} is reserved to protect the crystal structure). Therefore, minimum lithium stoichiometry (soc 100%) of $LiMn_2O_4$ is $stoich_{100} = 1.0 - 107/150 = 0.287$ and maximum lithium stoichiometry (soc 0%) is $stoich_0 = 1.0$ when irreversible loss is ignored. So, we can setup following functions using Fig. 1 with above relation.

$$U_i \begin{cases} = f_1(capa_i) \\ = f_2(stoich_i) \\ = f_3(soc_i) \end{cases} \quad \text{where} \quad \begin{cases} stoich_i = \dfrac{capa_i}{capa_{max,i}} \\ soc_i = \dfrac{stoich_i - stoich_{0,i}}{stoich_{100,i} - stoich_{0,i}} \end{cases} \tag{1}$$

Inversely, lithium stoichiometry or SOC can be found for the given equilibrium potential also by transforming the above functions as follows:

$$\begin{cases} f_1^{-1}(U_i) = capa_i \\ f_2^{-1}(U_i) = stoich_i = \dfrac{capa_i}{capa_{max,i}} = \dfrac{f_1^{-1}(U_i)}{capa_{max,i}} \\ f_3^{-1}(U_i) = soc_i = \dfrac{stoich_i - stoich_{0,i}}{stoich_{100,i} - stoich_{0,i}} = \dfrac{f_2^{-1}(U_i) - stoich_{0,i}}{stoich_{100,i} - stoich_{0,i}} \end{cases} \tag{2}$$

Note that the maximum capacity($capa_{max}$), the minimum lithium-stoichiometry ($stoich_0$), and the maximum lithium-stoichiometry($stoich_{100}$) of the active material i are known values. In order to get a full voltage profile of a blended-electrode with n-constituting active materials, we calculate accumulated capacity, lithium stoichiometry, and SOC of each material while sweeping equilibrium potential from U_{max} to U_{min} as follows:

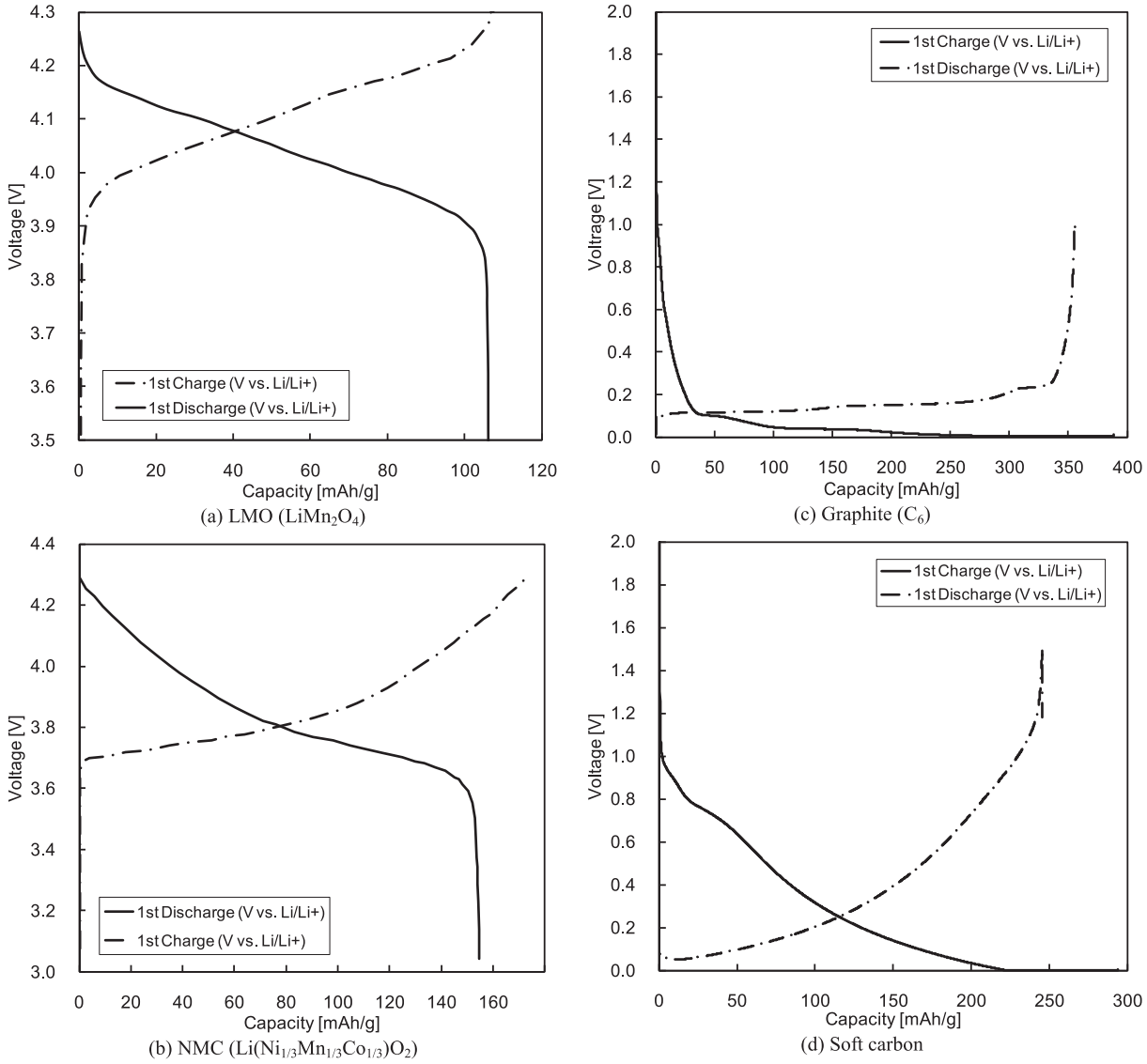

Fig. 1. Equilibrium voltage profile of pure active materials used for the present study.

$$
\begin{aligned}
capa_{\text{blend}} &= \sum_{i=1}^{n} capa_{\text{i}} \\
capa_{\text{i}} &= \xi_{\text{i}} capa_{\text{i}}(U) \quad \text{where} \quad \xi_{\text{i}} = \frac{capa_{\text{i}}}{capa_{\text{blend}}} \\
stoich_{\text{i}} &= stoich_{\text{i}}(U) \\
soc_{\text{i}} &= \frac{stoich_{\text{i}} - stoich_{0,\text{i}}}{stoich_{100,\text{i}} - stoich_{0,\text{i}}}
\end{aligned}
\tag{3}
$$

By applying the scheme explained above, equilibrium potentials of blended-electrodes can be generated as shown in Fig. 2. Positive blended-electrode made of $LiMn_2O_4$ (briefly 'LMO' from now) and $Li(Ni_{1/3}Mn_{1/3}Co_{1/3})O_2$ (briefly 'NMC' from now) gets more capacity with lowered overall potential when the fraction of NMC increases. Negative blended-electrodes made of graphite and soft carbon is simulated as shown in Fig. 2(b). Soft carbon has smoothly decreasing profile whereas graphite has step-decreasing profile due to lithium staging inside crystal layers (see Fig. 1). Therefore, when they are blended together, mixed potential profile is generated. As the present blended-electrode model has information of each constituting material, it is possible to extract several useful information of each material member from the model. Fig. 3(a) shows the contribution of each material member to the whole capacity production by the blended-electrode made of NMC (70%) and LMO (30%). Total capacity of the blended-electrode is about 143 mAh g^{-1}. NMC and LMO produces capacity together until the net capacity reaches 65 mAh g^{-1}. However, after the net capacity reaches 65 mAh g^{-1}, LMO does not make any capacity longer while NMC continues to produce more capacity until the net capacity reaches 143 mAh g^{-1}. Fig. 3(b) shows different view of capacity production of this blended-electrode. While the blended-electrode discharges from SOC 100%–0%, SOC of LMO component already reaches 0% when SOC of the blended-electrode is around 45%. Instead, NMC supports capacity production to the last of the discharging process. Note the SOC slope of NMC becomes stiffer after SOC of LMO reaches 0% in Fig. 3(b) since NMC solely covers the whole capacity production from this point on. Lithium stoichiometry status of each active material member can be analyzed as shown in Fig. 3(c). Starting from 0.3 at SOC 100%, lithium stoichiometry of LMO becomes almost 1.0 when SOC of the blended-electrode reaches 45%. In the case of NMC, lithium stoichiometry changes from 0.45 to 1.0 when SOC of the blended-electrode moves

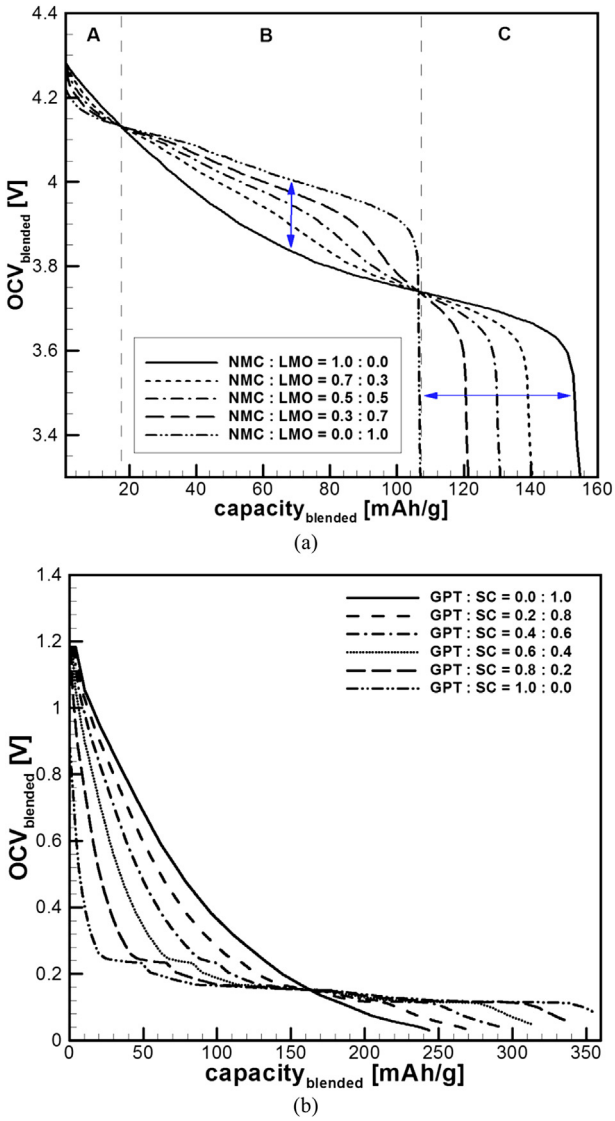

Fig. 2. Simulated equilibrium potentials of blended-electrodes according to blending ratio: (a) positive electrode composed of NMC and LMO, (b) negative electrodes made of graphite and soft carbon.

from 100% to 0%. dQ/dV profile is widely used for analyzing capacity production of an electrode according to voltage window. With the present blended-electrode model, one can separate dQ/dV of each material member from the total dQ/dV profile as shown in Fig. 3(d). It is easily identified that LMO produces capacity in the voltage range of 3.8–4.2 V whereas NMC covers the whole voltage window.

3. Dynamic model

Although the equilibrium model introduced above is useful for quickly predicting voltage profile and analyzing capacity production of a blended-electrode, it cannot simulate physical behavior of a battery under dynamics operating conditions. By combining the porous electrode theory [12–14] with the present blended-electrode model, the present dynamic blended-electrode model is developed. Fig. 4(a) shows the computation domain of the present model. Finite volume mesh is constructed in x-direction including negative electrode, separator, and positive electrode. Each finite volume has multiple active particles constituting a blended-electrode system. Spherical lithium intercalation equation is solved for each individual active particle. In addition, it is considered that those particles interact with each other to simulate physical behaviors of a blended-electrode as shown in Fig. 4(b).

3.1. Formulation

As the present model follows the framework of Newman group's [12,13], this paper briefly reviews the governing equations. Fig. 4(a) shows that there are three mathematical domains in the model. The following electrolyte-phase species equation is solved in the whole domain (anode, cathode, and separator).

$$\frac{\partial(\varepsilon c_e)}{\partial t} = \frac{\partial}{\partial x}\left(D_e^{eff}\frac{\partial c_e}{\partial x}\right) + \frac{1-t_+^0}{F}j^{Li} \quad \text{where} \quad D_e^{eff} = \varepsilon^{\tau} D_e \tag{4}$$

The left hand side term is the transient term, and the right hand side term consists of the diffusion term and the source term. Here, D_e^{eff} represents the effective lithium ion diffusivity of the electrolyte.

The electrolyte-phase potential equation is solved in the entire domain. Eq. (5) consists of the ohmic term and the ion-diffusion term with a source term representing the reaction current density j^{Li}. As the time scale of the potential is much smaller than that of Li-ion species equation, the transient term is neglected in Eq. (5).

$$\frac{\partial}{\partial x}\left(\kappa^{eff}\frac{\partial \phi_e}{\partial x}\right) + \frac{\partial}{\partial x}\left(\kappa_D^{eff}\frac{\partial}{\partial x}\ln c_e\right) = -j^{Li} \tag{5}$$

It is known that the ionic conductivity κ^{eff} is a strong function of the salt concentration, temperature, and material composition. Following relationship is used for finding the ionic conductivity of electrolyte composed of EC and EMC [19].

$$\begin{aligned}\kappa = {} & -3.37115 + 12.5608m - 7.89593m^2 + 3.51922m^3 \\ & - 1.15471m^4 + 18.1863x - 6.22756mx - 13.6916m^2x \\ & + 8.43904m^3x - 7.83732x^2 + 19.607mx^2 - 18.4529m^2x^2 \\ & - 30.6369x^3 + 29.2mx^3 - 0.0429918T + 0.180877mT \\ & - 0.0836202m^2T + 0.0230098m^3T + 0.195946Tx \\ & + 0.0676686mTx - 0.14134m^2Tx + 0.147429Tx^2 \\ & + 0.173059mTx^2 - 0.51634Tx^3 - 0.000223097T^2 \\ & + 0.000111233mT^2 + 0.0000495286m^2T^2 \\ & + 0.000952777T^2x + 0.00117334mT^2x \\ & - 0.000619157T^2x^2 - 3.46897 \times 1027T^3 - 2.75041 \\ & \times 1026mT^3 - 5.57653 \times 1026T^3x\end{aligned} \tag{6}$$

Note that m is electrolyte concentration and x is fraction of EC in the above equation.

The effective ionic conductivity is calculated by considering the porosity of the electrode as follows:

$$\kappa^{eff} = \varepsilon^{\tau}\kappa \tag{7}$$

κ_D^{eff} is the diffusive conductivity defined as follows [20]:

$$\kappa_D^{eff} = \frac{2RT\kappa^{eff}}{F}(t_+^0 - 1)\left\{1 + \frac{d\ln f_+}{d\ln c_e}\right\} \tag{8}$$

The solid-phase potential equation (or electron transport equation) which follows Ohm's law is solved in both electrodes.

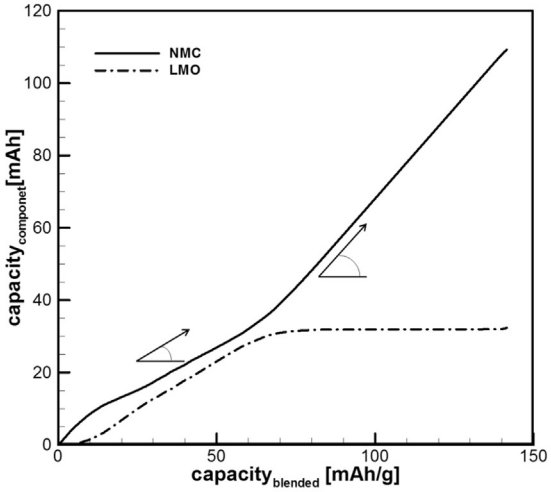

(a) Contribution of NMC and LMO to capacity production: LMO stops producing capacity when the net capacity production of the blended-electrode reaches 65mAh g^{-1} whereas NMC continues to produce capacity until the net capacity reaches the maximum value

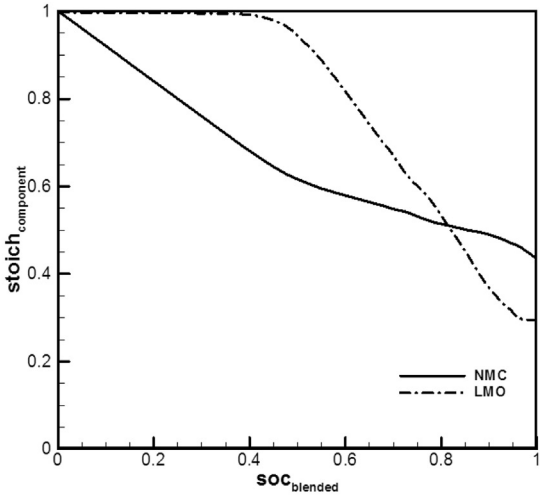

(c) Li-stoichiometry variation of each active material member (NMC and LMO) in the blended-electrode

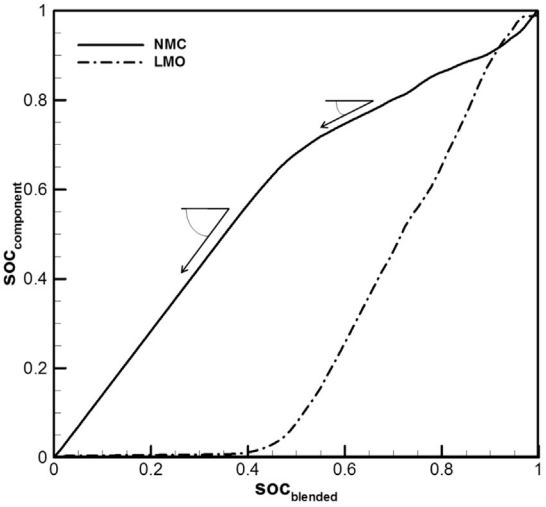

(b) SOC variation of each active material member (NMC and LMO) according to SOC of the blended- electrode: When the net SOC reaches 40%, SOC of LMO reaches 0% whereas remaining SOC of NMC is still 60%.

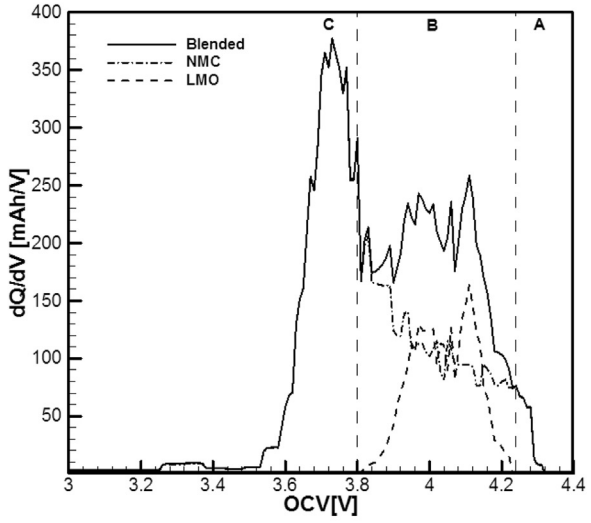

(d) Capacity production curves of the blended-electrode and the component materials

Fig. 3. Simulated result of a blended-electrode made of NMC (70%) and LMO (30%).

$$\frac{\partial}{\partial x}\left(\sigma^{\mathrm{eff}}\frac{\partial \phi_{\mathrm{s}}}{\partial x}\right) = j^{\mathrm{Li}} \tag{9}$$

where σ^{eff} is the effective electronic conductivity defined as $\sigma^{\mathrm{eff}} = (1-\varepsilon)^{\tau}\sigma$. Again, the transient term is ignored in the above equation where the electron transport is very fast compared to the Li-ion species transport.

As explained in the equilibrium model, open circuit potential (U_{i}) of each active material is defined as a function of lithium stoichiometry as follows:

$$stoich_{\mathrm{i}} = \left(c_{\mathrm{s}}/c_{\mathrm{s,max}}\right)_{\mathrm{i}} \tag{10}$$

Maximum lithium concentration $c_{\mathrm{s,max}}$ is theoretically determined and lithium concentration on an active particle c_{s} is calculated by solving a solid-phase lithium diffusion equation. In the present study, all active particles are assumed to be spherical. Therefore, solid-phase lithium concentration in the active particle is acquired by solving a spherical diffusion equation as follows:

$$\frac{\partial c_{\mathrm{s,i}}}{\partial t} = D_{\mathrm{s,i}}\frac{\partial^2 c_{\mathrm{s,i}}}{\partial r^2} + \frac{2D_{\mathrm{s,i}}}{r}\frac{\partial c_{\mathrm{s,i}}}{\partial r} \tag{11}$$

The above spherical equation is solved for each particle member constituting the blended-electrode. Solid-phase lithium diffusivity in active particles D_{s} is a function of temperature in this study. Eq. (12) shows lithium intercalation speed will increase at high temperature, which may result in improved C-rate performance of a cell.

$$D_{\mathrm{s,i}} = D_{\mathrm{s,i}}^{\mathrm{ref}} \cdot \exp\left\{\frac{E_{\mathrm{act}}}{R}\left(\frac{1}{T_{\mathrm{ref}}} - \frac{1}{T}\right)\right\} \tag{12}$$

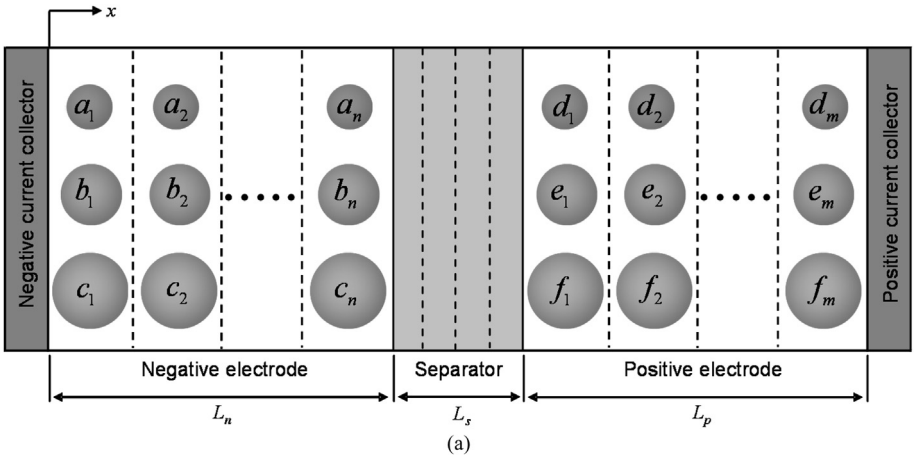

(a)

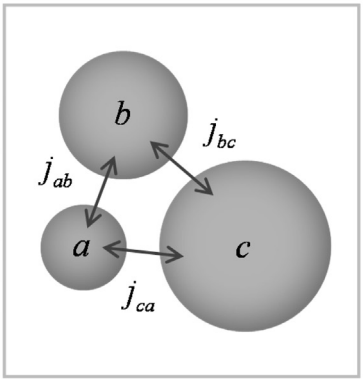

(b)

Fig. 4. Schematics of the present dynamic blended-electrode model: (a) Mathematical domain of the quasi-2D blended-electrode model, (b) Inter-particular relationship among three distinctly different active particles located in a single mathematical mesh domain.

Loading fraction ψ_i of each active material in a blended-electrode is expressed as

$$\psi_{\mathrm{i}} = \frac{\omega_{\mathrm{a,i}}}{\omega_{\mathrm{a}}} \quad \text{where} \quad \omega_{\mathrm{a}} = \sum_{\mathrm{i}=1} \omega_{\mathrm{a,i}} \tag{13}$$

Average density of active materials is

$$\rho_{\mathrm{a}} = \left(\sum_{i=1}^{n} \frac{\psi_i}{\rho_i} \right)^{-1} \tag{14}$$

Therefore, porosity of an electrode which has active material, binder, and conductive agent can be calculated as follows:

$$\varepsilon_{\pm} = 1 - \left(\frac{\omega_{\mathrm{a}}}{\rho_{\mathrm{a}} L_{\pm}} \right) - \left(\frac{\omega_{\mathrm{b}}}{\rho_{\mathrm{b}} L_{\pm}} \right) - \left(\frac{\omega_{\mathrm{c}}}{\rho_{\mathrm{c}} L_{\pm}} \right) \tag{15}$$

Specific interfacial area (a_s) which reflects the effective reaction area of each active material is defined as follows:

$$a_{\mathrm{s,i}} = N_{\mathrm{i}} \frac{A_{\mathrm{i}}}{L_{\pm}} \quad \text{where} \quad \begin{cases} A_{\mathrm{i}} = 4\pi r_{\mathrm{i}}^2 \\ \mathrm{V}_{\mathrm{i}} = \dfrac{4}{3}\pi r_{\mathrm{i}}^3 \\ N_{\mathrm{i}} = \dfrac{\omega_{\mathrm{i}}}{\rho_{\mathrm{i}} \mathrm{V}_{\mathrm{i}}} \end{cases} \tag{16}$$

Reaction kinetics at the interface between each active particle surface and electrolyte is assumed to follow the Butler–Volmer equation as follows:

$$j_{\mathrm{rxn,i}}^{\mathrm{Li}} = a_{\mathrm{s,i}} i_{\mathrm{o,i}} \left\{ \exp\left(\frac{\alpha_{\mathrm{a,i}} F}{RT} \eta_{\mathrm{i}} \right) - \exp\left(-\frac{\alpha_{\mathrm{c,i}} F}{RT} \eta_{\mathrm{i}} \right) \right\} \quad \text{where} \quad \eta_{\mathrm{i}} = \phi_{\mathrm{s}} - \phi_{\mathrm{e}} - U_{\mathrm{i}} \tag{17}$$

Exchange current density $i_{o,i}$ which is a function of lithium concentration in electrolyte phase and solid phase is expressed as follows [14]:

$$i_{\mathrm{o,i}} = \left[k (c_e)^{\alpha_{\mathrm{a}}} (c_{s,\max} - \overline{c}_s)^{\alpha_{\mathrm{a}}} (\overline{c}_s)^{\alpha_{\mathrm{c}}} \right]_i \tag{18}$$

When a blended-electrode consists of two different active particles (binary system), two different active particles will face each other and interactive reaction will occur to build equilibrium between them. The driving force of this interactive reaction is voltage difference between two active particles. If active particle 1 ($i = 1$) and active particle 2 ($i = 2$) constitute a blended-electrode, the interactive reaction current density can be defined as follows:

$$j_{12}^{\mathrm{Li}} = k_{12} (a_{s,12} i_{\mathrm{o},12}) \Delta U_{12} \cdot \exp\left\{ \frac{E_{\mathrm{act}}}{R} \left(\frac{1}{T_{\mathrm{ref}}} - \frac{1}{T} \right) \right\} \quad \text{where} \quad \Delta U_{12} = U_1 - U_2 \tag{19}$$

In Eq. (19), $a_{s,12}$ is specific surface area between active particles 1 and 2, which is assumed to be the smaller value between two particles. In the same way, exchange current density between two particles ($i_{o,12}$) is determined. k_{12} is reaction coefficient between two particles, which is an assumed value in the present study since it is difficult to measure this value. For each active particle,

$$\begin{aligned} j_1^{\mathrm{Li}} &= j_{\mathrm{rxn},1}^{\mathrm{Li}} + j_{12}^{\mathrm{Li}} \\ j_2^{\mathrm{Li}} &= j_{\mathrm{rxn},2}^{\mathrm{Li}} + j_{21}^{\mathrm{Li}} \end{aligned} \tag{20}$$

In each electrode, total reaction current is the sum of reaction current from each active material member. Therefore, the following description can be made.

$$j^{\mathrm{Li}} = \sum_{\mathrm{i}=1} j_{\mathrm{i}}^{\mathrm{Li}} = j_1^{\mathrm{Li}} + j_2^{\mathrm{Li}} \tag{21}$$

This total transfer current density is plugged into the governing equation Eqs. (4), (5), (9) and (11).

When the blended-electrode is a ternary system which has three distinctly different active particles, interactive reaction current densities among particles are

$$\begin{aligned} j_{12}^{\mathrm{Li}} &= k_{12}(a_{s,12} i_{\mathrm{o},12}) \Delta U_{12} \cdot \exp\left\{ \frac{E_{\mathrm{act}}}{R} \left(\frac{1}{T_{\mathrm{ref}}} - \frac{1}{T} \right) \right\} \quad \text{where} \quad \Delta U_{12} = U_1 - U_2 \\ j_{23}^{\mathrm{Li}} &= k_{23}(a_{s,23} i_{\mathrm{o},23}) \Delta U_{23} \cdot \exp\left\{ \frac{E_{\mathrm{act}}}{R} \left(\frac{1}{T_{\mathrm{ref}}} - \frac{1}{T} \right) \right\} \quad \text{where} \quad \Delta U_{23} = U_2 - U_3 \\ j_{31}^{\mathrm{Li}} &= k_{31}(a_{s,31} i_{\mathrm{o},31}) \Delta U_{31} \cdot \exp\left\{ \frac{E_{\mathrm{act}}}{R} \left(\frac{1}{T_{\mathrm{ref}}} - \frac{1}{T} \right) \right\} \quad \text{where} \quad \Delta U_{31} = U_3 - U_1 \end{aligned} \tag{22}$$

$$\begin{aligned} \dot{q}_+ &= \sum_{\mathrm{i}} (a_{\mathrm{s}} i_{\mathrm{o}})_{\mathrm{i}} (\phi_{\mathrm{s}} - \phi_{\mathrm{e}} - U_{\mathrm{i}}) + \sum_{\mathrm{i}} (a_{\mathrm{s}} i_{\mathrm{o}})_{\mathrm{i}} \left(T \frac{\mathrm{d}U}{\mathrm{d}T} \right)_{\mathrm{i}} + \sigma^{\mathrm{eff}} \nabla^2 \phi_{\mathrm{s}} + \kappa^{\mathrm{eff}} \nabla^2 \phi_{\mathrm{e}} + \kappa_{\mathrm{D}}^{\mathrm{eff}} \nabla \ln c_{\mathrm{e}} \nabla \phi_{\mathrm{e}} \\ \dot{q}_{\mathrm{s}} &= \kappa^{\mathrm{eff}} \nabla^2 \phi_{\mathrm{e}} + \kappa_{\mathrm{D}}^{\mathrm{eff}} \nabla \ln c_{\mathrm{e}} \nabla \phi_{\mathrm{e}} \\ \dot{q}_- &= \sum_{\mathrm{i}} (a_{\mathrm{s}} i_{\mathrm{o}})_{\mathrm{i}} (\phi_{\mathrm{s}} - \phi_{\mathrm{e}} - U_{\mathrm{i}}) + \sum_{\mathrm{i}} (a_{\mathrm{s}} i_{\mathrm{o}})_{\mathrm{i}} \left(T \frac{\mathrm{d}U}{\mathrm{d}T} \right)_{\mathrm{i}} + \sigma^{\mathrm{eff}} \nabla^2 \phi_{\mathrm{s}} + \kappa^{\mathrm{eff}} \nabla^2 \phi_{\mathrm{e}} + \kappa_{\mathrm{D}}^{\mathrm{eff}} \nabla \ln c_{\mathrm{e}} \nabla \phi_{\mathrm{e}} \end{aligned} \tag{25}$$

Current density of the blended-electrode becomes

$$j^{\mathrm{Li}} = \sum_{\mathrm{i}=1} j_{\mathrm{i}}^{\mathrm{Li}} = j_1^{\mathrm{Li}} + j_2^{\mathrm{Li}} + j_3^{\mathrm{Li}} \quad \text{where} \quad \begin{cases} j_1^{\mathrm{Li}} = j_{\mathrm{rxn},1}^{\mathrm{Li}} + j_{12}^{\mathrm{Li}} + j_{13}^{\mathrm{Li}} \\ j_2^{\mathrm{Li}} = j_{\mathrm{rxn},2}^{\mathrm{Li}} + j_{21}^{\mathrm{Li}} + j_{23}^{\mathrm{Li}} \\ j_3^{\mathrm{Li}} = j_{\mathrm{rxn},3}^{\mathrm{Li}} + j_{31}^{\mathrm{Li}} + j_{32}^{\mathrm{Li}} \end{cases} \tag{23}$$

In the same way, the present model can be extended to any blended electrode system with N-different active particles.

As the physical behavior of a cell is strongly affected by temperature, it is necessary to find the cell temperature, especially under high C-rate case where it is difficult to maintain constant temperature. It is assumed that temperature in the cell is same everywhere due to the small scale of the present model. Therefore, the following lumped heat equation is coupled with the present model.

$$mc_{\mathrm{p}} \frac{\mathrm{d}T}{\mathrm{d}t} = hA_{\mathrm{surf}}(T - T_{\mathrm{amb}}) + \dot{q} \tag{24}$$

Heat source term $\dot{q}$ consists of the followings [21].

Note each electrode has reaction heat, electronic ohmic heat, ionic ohmic heat whereas separator has only ionic ohmic heat in the above expression.

Governing equations with boundary conditions for the present model are summarized in Table 1. The model is incorporated into FORTRAN and solved by finite volume method.

Table 1
Governing equations and boundary conditions of the Li-ion cell model.

Description	Conservation equation	Boundary condition
Charge (electrolyte phase)	$\frac{\partial}{\partial x}\left(\kappa^{\mathrm{eff}} \frac{\partial \phi_{\mathrm{e}}}{\partial x}\right) + \frac{\partial}{\partial x}\left(\kappa_{\mathrm{D}}^{\mathrm{eff}} \frac{\partial}{\partial x} \ln c_{\mathrm{e}}\right) = -j^{\mathrm{Li}}$	$\left.\frac{\partial \phi_{\mathrm{e}}}{\partial x}\right\|_{x=0} = \left.\frac{\partial \phi_{\mathrm{e}}}{\partial x}\right\|_{x=L} = 0$
Charge (solid phase in electrode matrix)	$\frac{\partial}{\partial x}\left(\sigma^{\mathrm{eff}} \frac{\partial \phi_{\mathrm{s}}}{\partial x}\right) = j^{\mathrm{Li}}$	$-\sigma_-^{\mathrm{eff}} \left.\frac{\partial \phi_{\mathrm{s}}}{\partial x}\right\|_{x=0} = \sigma_+^{\mathrm{eff}} \left.\frac{\partial \phi_{\mathrm{s}}}{\partial x}\right\|_{x=L} = \frac{I}{A}$
		$-\sigma_-^{\mathrm{eff}} \left.\frac{\partial \phi_{\mathrm{s}}}{\partial x}\right\|_{x=L_n} = \sigma_+^{\mathrm{eff}} \left.\frac{\partial \phi_{\mathrm{s}}}{\partial x}\right\|_{x=L_{n+s}} = 0$
Species (electrolyte phase)	$\frac{\partial(\varepsilon_{\mathrm{e}} c_{\mathrm{e}})}{\partial t} = \frac{\partial}{\partial x}\left(D_{\mathrm{e}}^{\mathrm{eff}} \frac{\partial c_{\mathrm{e}}}{\partial x}\right) + \frac{1 - t_+^0}{F} j^{\mathrm{Li}}$	$\left.\frac{\partial c_{\mathrm{e}}}{\partial x}\right\|_{x=0} = \left.\frac{\partial c_{\mathrm{e}}}{\partial x}\right\|_{x=L} = 0$
Species (solid phase in particles)	$\frac{\partial c_{\mathrm{s}}}{\partial t} = D_{\mathrm{s}} \frac{\partial^2 c_{\mathrm{s}}}{\partial r^2} + \frac{2D_{\mathrm{s}}}{r} \frac{\partial c_{\mathrm{s}}}{\partial r}$	$c_{\mathrm{s}} = c_{\mathrm{s},0}$ at $t = 0$
		$D_{\mathrm{s}} \frac{\partial c_{\mathrm{s}}}{\partial r} = 0$ at $r = 0$
		$D_{\mathrm{s}} \frac{\partial c_{\mathrm{s}}}{\partial r} = \frac{j^{\mathrm{Li}}}{F}$ on particle surface
Energy	$mc_{\mathrm{p}} \frac{\mathrm{d}T}{\mathrm{d}t} = hA_{\mathrm{surf}}(T - T_{\mathrm{amb}}) + \dot{q}$	

Table 2
Simulation result of NMC/LMO blended-electrode according to the material composition.

Total loading (mg cm^{-2})	NMC loading (mg cm^{-2})	LMO loading (mg cm^{-2})	NMC fraction (%)	Electrode capacity (mAh cm^{-2})
16.0	0.0	16.0	0	1.630
16.0	4.8	11.2	30	1.863
16.0	8.0	8.0	50	2.096
16.0	11.2	4.8	70	2.212
16.0	16.0	0.0	100	2.445

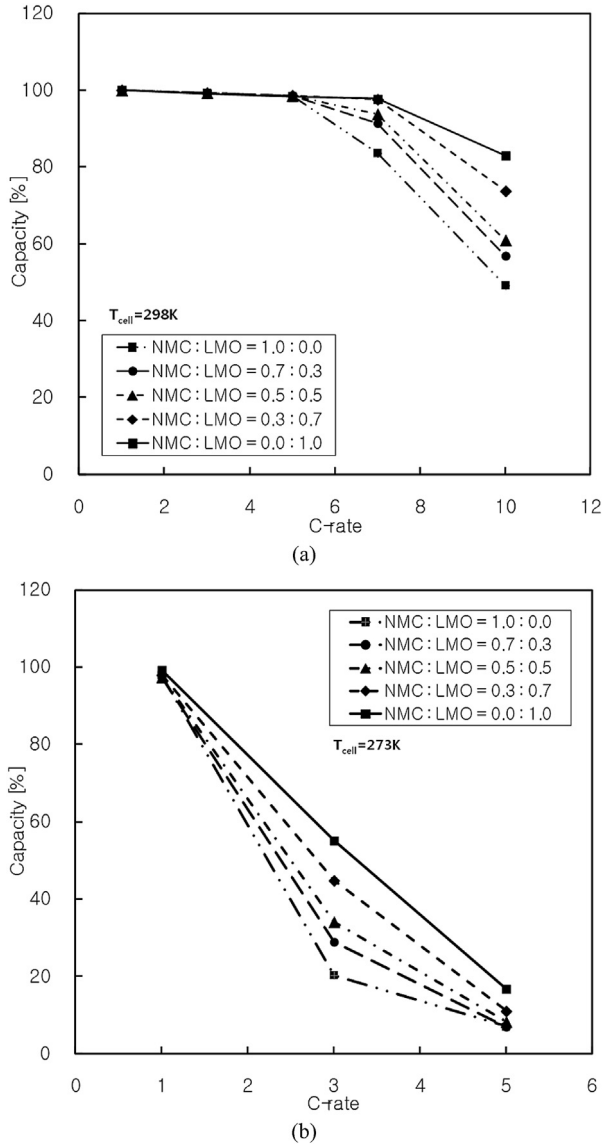

Fig. 5. Simulated C-rate performance of NMC/LMO blended-electrode: (a) $T_{cell} = 298$ K, (b) $T_{cell} = 273$ K.

Table 3
Active material composition of full-cells constructed for the present study.

Full-cell no.	Cathode		Anode	
	NMC (%)	LMO (%)	Graphite (%)	Carbon (%)
1	70.0	30.0	90.0	10.0
2	50.0	50.0	90.0	10.0
3	30.0	70.0	5.0	95.0

3.2. Result and discussion

LMO and NMC are widely used active materials for Li-ion cells. LMO has advantage of fast lithium intercalation due to spinel structure along with relatively high operational voltage, which enables a Li-ion cell to produce high power. For this reason, LMO will be a good choice as positive material for HEV application. In contrast, NMC has advantage of larger theoretical capacity (277 mAh g^{-1}) compared to LMO (150 mAh g^{-1}) although lithium intercalation rate is a bit lower compared to LMO. Therefore, it is reasonable to think that a blended-electrode composed of both NMC and LMO has intermediate characteristics between them. In other words, it is possible to acquire both advantages from NMC and LMO with a blended-electrode.

Discharging performance of NMC/LMO blended-electrodes is simulated using the dynamic model according to five blending cases as listed in Table 2. Calculation result shows net electrode capacity linearly increases according to increment of NMC fraction. This result is almost identical with the result of equilibrium model (see Fig. 2(a)). Effect of blending ratio on C-rate capability is shown in Fig. 5. It is clear that blending more LMO leads to improved C-rate capability due to fast lithium diffusion in LMO particles, especially under high C-rate condition over 7C. In addition, LMO helps a cell produce more power or large current at low temperature.

In order to validate the present dynamic model, three different full cells with different electrode compositions are built as listed in Table 3. Baseline model parameters used for the simulation are listed in Table 4. Three cells are simulated under the given test conditions, and compared with experimental result as shown in Fig. 6. By blending different active materials, each cell shows distinctly different voltage profiles. Cell #1 and cell #2 have most of their capacity production in the voltage window of 4.1–3.4 V whereas cell #3 shows slowly decreasing voltage profile between 4.1 and 2.8 V. This result came from anode material selection (graphite vs. amorphous carbon). As cell #1 and cell #2 share the same anode, difference between them comes from the cathode

Table 4
Baseline model parameters.

Parameter	Unit	Value	Note
Radius of NMC	μm	4.5	Measured
Radius of LMO	μm	7.5	Measured
Radius of graphite	μm	7.5	Measured
Radius of soft carbon	μm	3.8	Measured
Li-ion diffusivity of NMC	cm^2 s^{-1}	5.5×10^{-10}	Fitted
Li-ion diffusivity of LMO	cm^2 s^{-1}	2.5×10^{-9}	Fitted
Li-ion diffusivity of graphite	cm^2 s^{-1}	4.5×10^{-10}	Fitted
Li-ion diffusivity of soft carbon	cm^2 s^{-1}	1.7×10^{-9}	Fitted
Thickness of negative current collector	μm	10.0	Measured
Thickness of positive current collector	μm	20.0	Measured
Thickness of negative electrode	μm	50.0	Measured
Thickness of positive electrode	μm	55.0	Measured
Thickness of separator	μm	25.0	Measured
Porosity of negative electrode		0.28	Measured
Porosity of positive electrode		0.25	Measured
Porosity of separator electrode		0.37	Measured
Ionic conductivity in electrolyte	S cm^{-1}	Eq. (6)	From ref. [6]
Transference number		0.363	
Faraday's constant (F)	C mol^{-1}	96,487	
Li-ion diffusivity in electrolyte	cm^2 s^{-1}	2.5×10^{-6}	From ref. [6]
Average concentration of Li-ion in electrolyte	M	1.0	
Matrix electronic conductivity (positive)	S cm^{-1}	0.062	Measured
Matrix electronic conductivity (negative)	S cm^{-1}	0.1	Measured

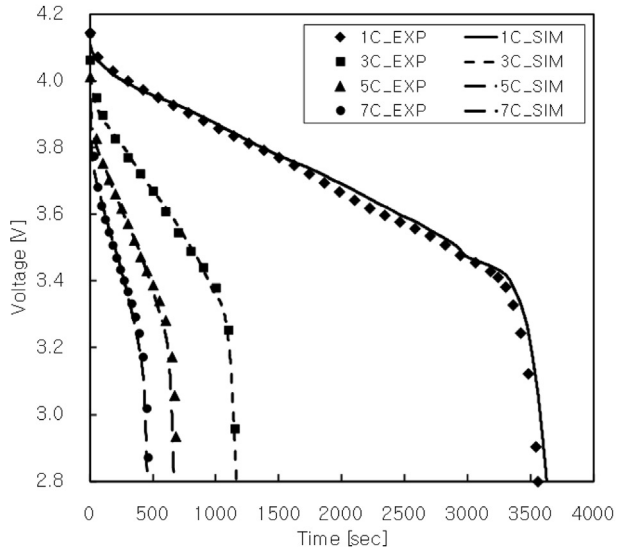

(a) Discharging profiles of full-cell #1

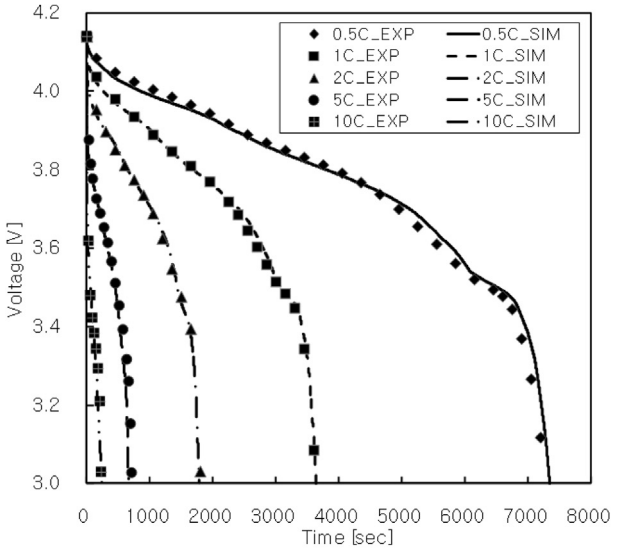

(b) Discharging profiles of full-cell #2

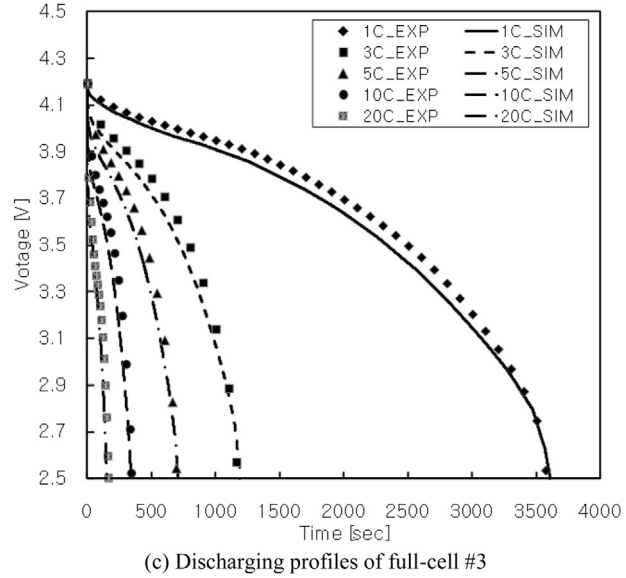

(c) Discharging profiles of full-cell #3

Fig. 6. Experimental validation of Li-ion cells with blended-electrodes (full-cell #1, #2, #3).

side. Discharging simulation of 10C was successful with cell #2 which has large LMO fraction whereas cell #1 showed maximum 7C discharging performance with the present model. This result confirms that using much amount of fast diffusion material in the electrode is beneficial for getting high power from a lithium-ion cell although there are other factors to control C-rate performance of a cell such as electrode thickness. Cell #3 achieved very high C-rate performance (20C) compared to other cells. This high power performance was possible with the following three reasons. First, the cathode consists of large amount of manganese spinel and the most of active material fillings the anode is amorphous carbon which has fast solid-phase lithium diffusion speed. Second, electrode thickness of cell #3 is less thick (about 60%) compared to cell #1 and #2. Third, both electrode of cell #3 is very porous compared to the other cells, which means amount of active material loading is low. Consequently, energy density of cell #3 is lower than the other cells. In contrast, opposite approaches of the above three methods should be considered when a cell with high energy density is designed. High energy density cells can be applied to energy storage systems (ESS) which does not require high power capability as xEVs do. For automotive applications, cell #1 and #2 will be

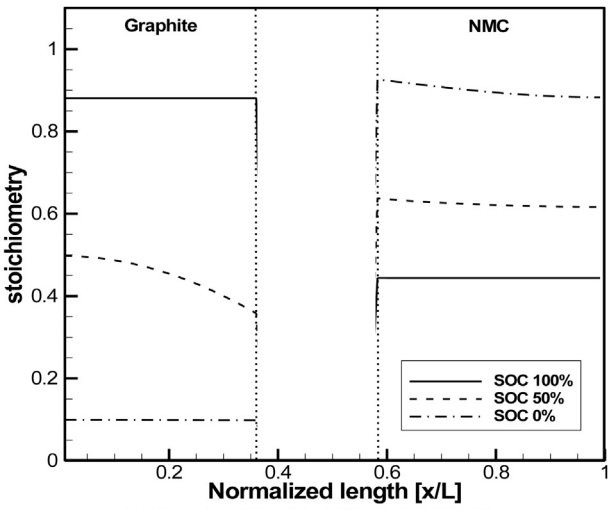

(a) Negative (Graphite) || Positive (NMC)

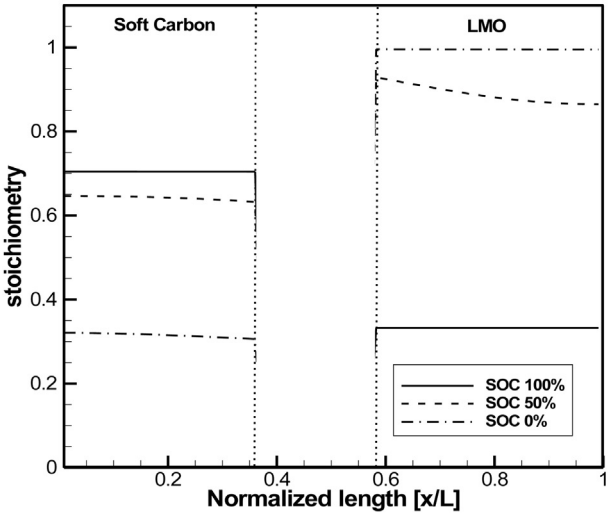

(b) Negative (Soft carbon) || Positive (LMO)

Fig. 7. Li-stoichiometry profiles of each active material in full-cell #1 during 3C discharging.

appropriate for PHEV or EV, whereas cell #3 will be a good choice for HEV which require high power than large amount of energy.

It is possible to analyze physical behavior of each active material member in a cell with the present model. Fig. 7 show lithium stoichiometry of each active material in cell #1 under discharging condition. It is observed that lithium stoichiometry window of graphite is wider than that of carbon in the anode while lithium stoichiometry window of LMO is wider than that of NMC in the cathode.

When a blended-electrode has several constituting active materials with quite different physical properties such as temperature dependency of lithium-ion diffusivity, the voltage profile may significantly change according to the operating condition. Fig. 8 presents simulated discharging profiles of a lithium-ion cell with a blended-positive electrode (NMC 85% and LPF 15%) and a negative electrode (graphite 100%). Under the mild operating condition (room temperature, 298 K), discharging ends up with negative-limiting condition and the positive voltage plateau of LPF shows up lately (see Fig. 8(a)). On the other hand, the positive voltage plateau of LPF shows up early and the discharging ends up with positive-limiting condition when the cell operates at low temperature (see Fig. 8(b)). In this simulation case, it was assumed that the temperature dependency of lithium-ion diffusivity in NMC particle is stronger than that of graphite particle. Therefore, solid-phase mass-transport in NMC particle is getting slower than that of graphite particle at low temperature. As the lithium concentration on the surface of NMC particle is quickly saturated due to slow lithium intercalation, operation of LPF starts up earlier under the low temperature condition than the mild operating condition. In other words, the length of span A and B strongly depends on the material properties of the constituting active particles, which can be easily predicted with the present dynamic model.

Another simulation examples of lithium-ion cells with blended-electrodes are shown in Fig. 9. According to the blending ratio and negative/positive ratio, numerous combinations of cells can be constructed. When material properties of each active material are prepared, characteristics and physical behavior of those cells can be

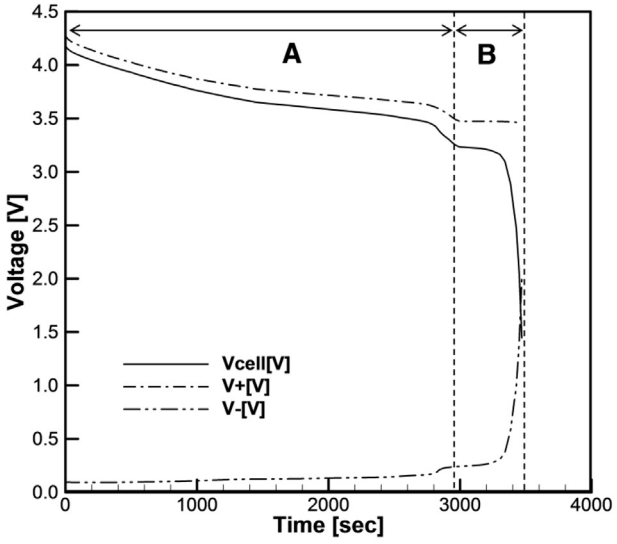

(a)

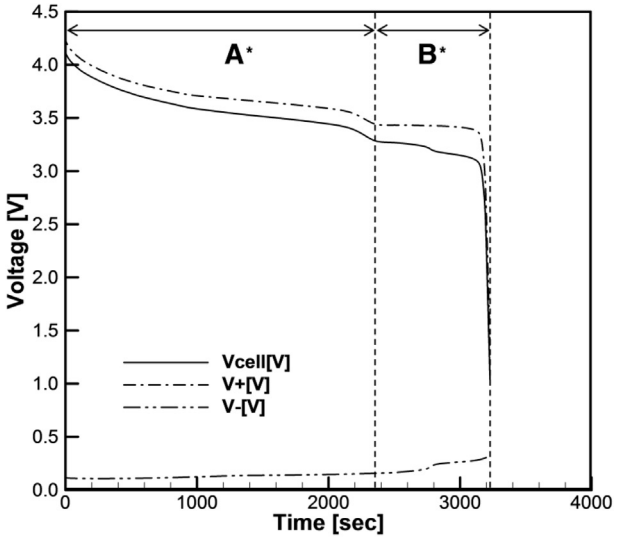

(b)

Fig. 8. Simulated 1C discharging profiles of a Li-ion cells with positive electrode composed of NMC 85%//LFP 15% and negative electrode composed of graphite 100%, (a) $T = 298$ K, (b) $T = 273$ K.

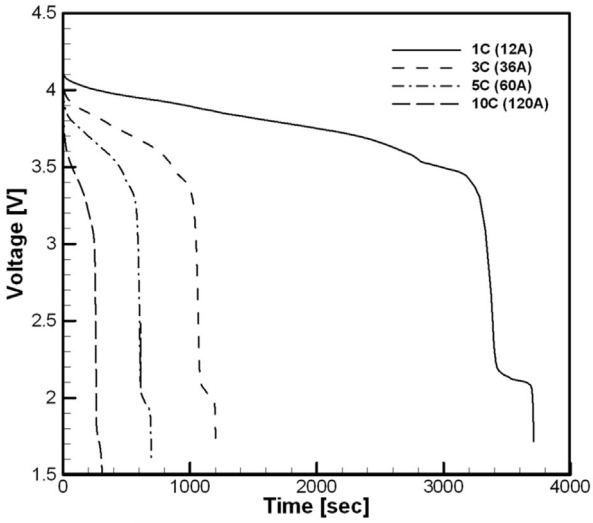

(a) Discharging profiles of a Li-ion cell with positive electrode composed of NMC 50% // LMO 50% and negative electrode composed of graphite 90% // LTO 10%

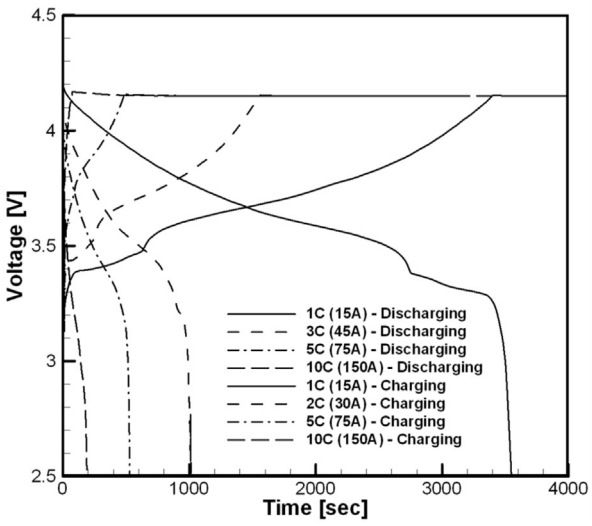

(b) Discharging profiles of a Li-ion cell with positive electrode composed of NMC 70% // LFP 30% and negative electrode composed of graphite 100%

Fig. 9. Simulated result of various Li-ion cells with blended-electrodes.

predicted with the present model. This will eventually expedite cell development process which usually takes much time and effort.

4. Conclusion

Two mathematical models of lithium-ion cells with blended-electrodes are developed. First, the equilibrium model can simulate any combination of active materials in a blended-electrode by a quick and easy method. The equilibrium model enables us to decompose a blended-electrode into each active material, analyzing steady-state characteristics of each constituting member such as voltage window, and lithium stoichiometry. Second, the physics-based dynamic model can conduct simulation under various operating conditions such as C-rate and temperature by solving physico-chemical governing equations. Simulation results show good agreement with the experiment data, confirming that the present model is useful for checking candidate active material compositions at the early stage of battery development.

Nomenclature

Acronyms and abbreviations

a_s	active surface area per electrode unit volume (cm^{-1})
A	area (cm^2)
c	concentration of lithium (mol cm^{-3})
c_p	specific heat (J K^{-1})
capa	capacity
D	diffusivity of lithium (cm^2 s^{-1})
E_{act}	activation energy
h	heat transfer coefficient (W cm^{-2} K^{-1})
i_0	exchange current density (A cm^{-2})
I	applied current (A)
j	volumetric current density (A cm^{-3})
k	reaction coefficient
L	thickness (cm)
m	mass (g)
N	number of active particles
r	radial coordinate, radius (cm)
R	universal gas constant (8.314 J mol^{-1} K^{-1})
soc	state of charge
stoich	lithium stoichiometry
t	time (sec)
t_+^o	transference number of lithium ion with respect to the velocity of solvent
T	temperature (K)
V	volume (cm^3)
x	thickness coordinate (cm)
U	open circuit potential (V)
$\dot{q}$	heat source (W)

Greek letters

α_a, α_c	anodic and cathodic transfer coefficient for an electrode reaction
ε	porosity
ϕ	potential (V)
η	surface overpotential of an electrode reaction (V)
κ	ionic conductivity (S cm^{-1})
κ_D	diffusive conductivity of a species (A cm^{-1})
ρ	density
σ	electronic conductivity (S cm^{-1})
τ	Bruggeman tortuosity exponent
ψ	loading fraction
ω	loading amount (g cm^{-2})
ξ	capacity fraction

Superscripts and subscripts

a	active material
b	binder
amb	ambient
c	conductive agent
diff	diffusion
e	electrolyte phase
eff	effective
eq	equilibrium
i	ith member
Li	lithium
ref	reference
rxn	reaction
s	solid phase
surf	surface

References

[1] S.Y. Chung, J.T. Bloking, Y.M. Chiang, Nat. Mater. 1 (2002) 123.
[2] Y. Xia, M. Yoshio, H. Noguchi, Electrochem. Acta 52 (2006) 240.
[3] C.R. Sides, F. Croce, V.Y. Young, C.R. Martin, B. Scrosatt, Electrochem. Solid State Lett. 8 (2005) A484.
[4] Z. Bakenov, I. Taniguchi, in: 216th Meeting of the Electrochemical Society, 2009.
[5] T. Numata, C. Amemiya, T. Kumeuchi, M. Shirakata, M. Yonezawa, J. Power Sources 97-98 (2001) 358.
[6] A. Manthiram, W. Choi, Electrochem. Solid State Lett. 10 (2007) A228.
[7] S.T. Myoung, M.H. Cho, H.T. Hong, T.H. Kang, C.S. Kim, J. Power Sources 146 (2005) 222.
[8] J.W. Fergus, J. Power Sources 195 (2010) 939.
[9] J.F. Whitacre, K. Zaghib, W.C. West, B.V. Ratnakumar, J. Power Sources 177 (2008) 528.
[10] R. Darling, J. Newman, J. Electrochem. Soc. 144 (1997) 4201.
[11] P.M. Gomadam, D.R. Merritt, E.R. Scott, C.L. Schmidt, P.M. Skarstad, J.W. Weidner, J. Power Sources 174 (2007) 628.
[12] M. Doyle, T.F. Fuller, J. Newman, J. Electrochem. Soc. 140 (1993) 1526.
[13] T.F. Fuller, M. Doyle, J. Newman, J. Electrochem. Soc. 141 (1994) 1.
[14] W.B. Gu, C.Y. Wang, in: Lithium Batteries, PV99–25, 748, The Electrochemical Society Proceeding Series, Pennington, NJ, 2000.
[15] P. Albertus, J. Newman, in: 214th Meeting of the Electrochemical Society, 2008.
[16] P. Albertus, J. Newman, in: 215th Meeting of the Electrochemical Society, 2009.
[17] P. Albertus, J. Christensen, J. Newman, J. Electrochem. Soc. 156 (2009) A606.
[18] S. Jung, D. Kang, J. Power Sources 248 (2014) 498.
[19] M.S. Ding, K. Xu, S.S. Zhang, K. Amine, G.L. Henrikent, T.R. Jow, J. Electrochem. Soc. 148 (2001) A1196.
[20] J. Newman, K.E. Thomas-Alyea, Electrochemical Systems, third ed., Wiley Inter-Science Inc., Hoboken, NJ, 2004.
[21] L. Rao, J. Newman, J. Electrochem. Soc. 144 (1997) 2697.